3-D Time-domain Full Waveform Inversion of a Valhall OBC dataset

*Faqi Liu [1] *, Lluis Guasch [2] , Scott A. Morton [1] , Mike Warner [2] , Adrian Umpleby [2] , Zhaobo Meng [3] , Stuart Fairhead [1] , and Steve Checkles [1]*

[1] Hess Corporation, 1501Mckinney Street, Houston, TX 77010; [2] Imperial College, London; [3] In-Depth Geophysical Inc, Houston, TX

Summary

By minimizing the difference between synthetic and field data sets, full waveform inversion (FWI) can produce high resolution and high fidelity earth model parameters that are not resolvable by commonly used ray-based tomography. In this paper, we share our experience on applying 3-D acoustic time-domain full waveform inversion to an OBC data set collected over Valhall field in North Sea.

Introduction

Ray-based tomography has been the main algorithm in deriving velocity models. However, this image-domain method can only produce a smooth result that is mostly used for depth imaging; it is incapable of sensing the small scale structures in the earth parameters.

Full waveform inversion, on the other hand, is a data-domain (time or frequency) algorithm, which can derive a fine-scale model such that the synthetic data can best match the recorded field data. FWI is typically casted as a minimization problem. The methods to solve such inversion problems can be classified in two general groups: one is the global optimization algorithm, like simulated annealing (Sen and Stoffa, 1991), genetic algorithms (Stoffa and Sen, 1991), etc. These methods have been employed in many inversion related applications (Landa, et. al., 1989, Ma, 2002), but for FWI, their efficiency is limited by the large dimensionality involved in a typical problem; the second category is an iterative approach, which is often associated with the computation for the gradient of the objective function, like the steepest decent method, conjugate gradient method, etc. In FWI, the gradient is computed by crosscorrelating a forwarded extrapolated source wavefield with a backward propagated residual of the synthetic and field data in a manner similar to reverse-time migration. This method can be implemented in either the time- (Tarantola, 1984, Warner, et al., 2008) or the frequency-domain (Pratt, et. al, 1998). There is no theoretical advantage for either approach compared to the other, but FWI in time-domain is easier for quality control.

The major difficulty for the gradient based iterative inversion comes from the existence of local minima of the objective function (Bunks, et al, 1995), which poses strict constraint for the accuracy of the simulated data, i.e., no cycle skipping between the synthetic and field data, which mostly challenges its applications.

The Valhall field has been in production since 1982. A permanent seismic array, for "life of field seismic" surveys (LoFS), was installed on the ocean floor in 2003. Since then, many seismic surveys have been acquired. More detailed information about the LoFS surveys and the Valhall field can be found in Barkved, et. al., (2010). Frequency-domain FWI has been applied to Valhall datasets in both 2D and 3D from different surveys (Sirgue, et. al., 2009, Barkved, et. al., 2010, Prieux, et. al., 2010). Here, we discuss our application of 3-D time-domain acoustic full waveform inversion to a dataset collected at LoFS survey 12. The derived model has successfully improved the image; in addition, the model itself also exhibits many geological features: channels in the first few hundred meters and a clear delineation of the gas cloud below 1 km in depth. Our experiment concludes that an accurate starting velocity model and careful quality control at each step are crucial for FWI to be successful.

Theory

Full waveform inversion is a data matching algorithm. Mathematically, it is represented as a minimization problem for an objective function defined as

$$E(m) = \sum_{s,r} \left\| d(t,s,r) - d_{syn}(t,s,r,m) \right\|_{L^2} \qquad (1)$$

$E(m)$ measures the difference between the recorded data $d(t,s,r)$ and the synthetic one $d_{syn}(t,s,r,m)$, at source s, receiver r and using the model m, which will be solved such that $E(m)$ reaches its global minimum. Equation 1) is generally solved using a gradient-based method in either the time- or frequency-domain. We use the following time–domain iterative scheme, with the steepest decent method, as follows: for an initial velocity model m, let $m_0 = m$,

$$m_{k+1} = m_k - \lambda_k h_k , \qquad (2a)$$

DOI http://dx.doi.org/10.1190/segam2012-1105.1

$$h_k = \frac{2}{m^3}\sum_s \left(\frac{\partial}{\partial t} r_k^s \frac{\partial}{\partial t} p_k^s \right), \quad (2b)$$

$$\lambda_k = \frac{\sum_s \delta E_k^s E_k^s}{\sum_s \delta E_k^s \delta E_k^s}, \quad (2c)$$

$$E_k^s = E^s(m_k) = \sum_r \left\| d(t,s,r) - d_{syn}(t,s,r,m_k) \right\|_{L^2}, \quad (2d)$$

$$\delta E_k^s = \bar{E}_{k+1}^s - E_k^s, \quad \bar{E}_{k+1}^s = E^s(m_k - h_k).$$

p_k^s, r_k^s is the forward extrapolated source and backward extrapolated data residual for shot gather s using current model m_k, h_k is the gradient of the objective function.

Application to a Valhall dataset

We applied FWI to the pressure data from the multi-component LoFS survey 12. This installation consists of about 2500 receivers sitting on the ocean floor in about 70 meters of water and covering an area about 45 km^2. We used only a fraction of the data consisting of approximately 400 receivers spaced at about 200m apart.

The gradient-based inversion problem in equation 1) and 2) is nonlinear, the solution is non-unique. To ensure it converges to its global minima, the synthetic shot gathers are required to be accurate enough without cycle skipping comparing to the field shot gathers. For that purpose, it is very important to preserve the low frequency content as much as one can in the data and have an accurate initial velocity model to start with, since this is, in fact, a measure of the effective wavelength. In addition, having a source wavelet that matches with that in the field data is also crucial (Vigh and Starr, 2008, Virieux and Operto, 2009). All these requirements are easy to be satisfied for a synthetic data set, but can be difficult in reality. In addition, the strong multiples in the shallow part of the data makes the process challenging.

Preprocessing: Minimum preprocessing has been applied to the raw shot gathers before input to FWI other than proper denoising and low-pass filtering up to 7 Hz. The FWI is applied starting at 3 Hz and gradually increasing the frequency in $1/4$ Hz increments. Reciprocity has been applied to generate common-receiver gathers as the input instead of original shot gathers, which significantly reduces the computation in each iteration. The objective function in equation 1) attempts to minimize the difference in both amplitude and phase of the field and synthetic data. However, the problem is set up to only invert the velocity, the density is computed using Gardner's empirical equation during the simulation. Amplitude balancing in a trace by trace manner is important to mitigate the difference.

Wavelet Extraction: It is a common practice to derive an effective wavelet from water-bottom reflection in marine data sets. Here, we extracted a wavelet from a raw near offset trace as shown in Fig 1a). As it is recorded on the sea floor, the first event is, in fact, a mixture of source side ghost, direct wave and reflection at the water bottom. As expected, the trace also has free surface multiples. An effective wavelet is derived after the removal of multiple and ghost and a low-pass filtering to the same frequency band as the input data (Fig. 1b). Its applicability is confirmed by carefully comparing a synthetic shot gather with the recorded one before inversion. It is also verified by comparing the synthetic gathers using the initial and the FWI model against the field gather as shown in Fig 1c), 1d) and 1e). The nice match between the field gather (Fig 1c) and the synthetic one using the inverted model (Fig 1d) indicates that the wavelet indeed is a reasonable approximation that makes the inversion converge.

Starting velocity model: It is well understood that an "accurate" initial velocity model is important for FWI to converge to its global minima. A ray-based tomography has been carefully applied to build the starting velocity model, which is smooth as one can expect (Fig 2a). Some common imaging gathers of Kirchhoff migration using this model are shown in Fig 2b), from which we can see that the gathers are reasonably flat, even though the continuity of the events down the deep in the stack volume has not been established (see Fig 2c).

Inversion results: After FWI, a detailed model is constructed as shown in Fig 3a), compared to the same line in the starting model (Fig 2a), especially at its shallow part. The common imaging gathers at the same locations as Fig 2b) are generated using this new model (Fig 3b), and the new image section corresponding to Fig 2c) is given in Fig 3c), where the image is significantly improved in the middle and a continuous event at the deeper section is successfully constructed. Many of the common imaging gathers in Fig 3b) are flattened, but some of them do not have significant

DOI http://dx.doi.org/10.1190/segam2012-1105.1

difference because the curvature-based tomography is insensitive to small scale model perturbation, which is one of the main reasons that a velocity model derived using this method is usually smooth. The accuracy of the inverted model can also be confirmed by comparing the field data (Fig 1c) with the synthetic one using the inverted model (Fig 1d) and that from the initial model (Fig 1f). It is clear that the model after FWI generates a gather that matches with the field data in much greater detail, but the synthetic data using the initial model fails in such a comparison. In addition to the improvement in seismic data, FWI also resolves many geological features as shown in Fig 4 and Fig 5, where, Fig 4b) is a depth slice of the inverted model at a shallow depth, detailed channel structures are inverted properly. Fig 5b) is a depth slice at a deeper section, which clearly shows the sharp boundary of the gas cloud. Both features are invisible in the corresponding depth slices of the initial model as shown in Fig 4a) and Fig 5a), respectively.

Acknowledgements

We thank our colleagues Peter Barnhill, Xiaochun Ma and Ben Vaughn for their help in this project. We also thank Hess Corporation and our Valhall partner BP (the operator) for permission to publish this paper.

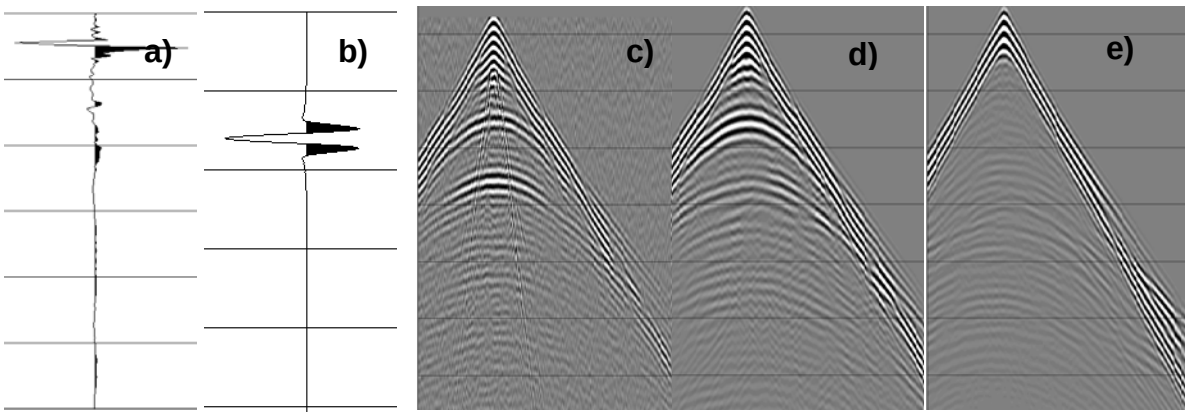

Fig 1) a) a raw near offset trace, b) a wavelet derived from 1a), it is shifted 700 ms down the trace; c) a field shot gather input to FWI; d) a synthetic shot gather using the wavelet and FWI inverted model; f) a synthetic shot gather using the same wavelet but initial velocity model. Note that, a) and b) are not plotted in the same scale as they are of significantly different frequency content.

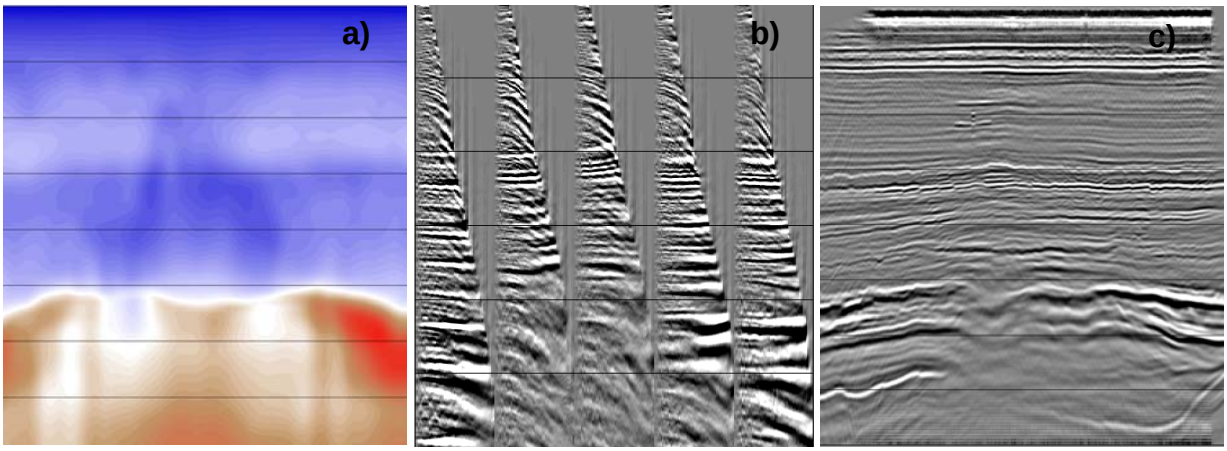

Fig 2: a) One inline section in the initial velocity model before FWI; b) some common imaging gathers of Kirchhoff migration using the initial model; c) the migrated section using the initial model.

DOI http://dx.doi.org/10.1190/segam2012-1105.1

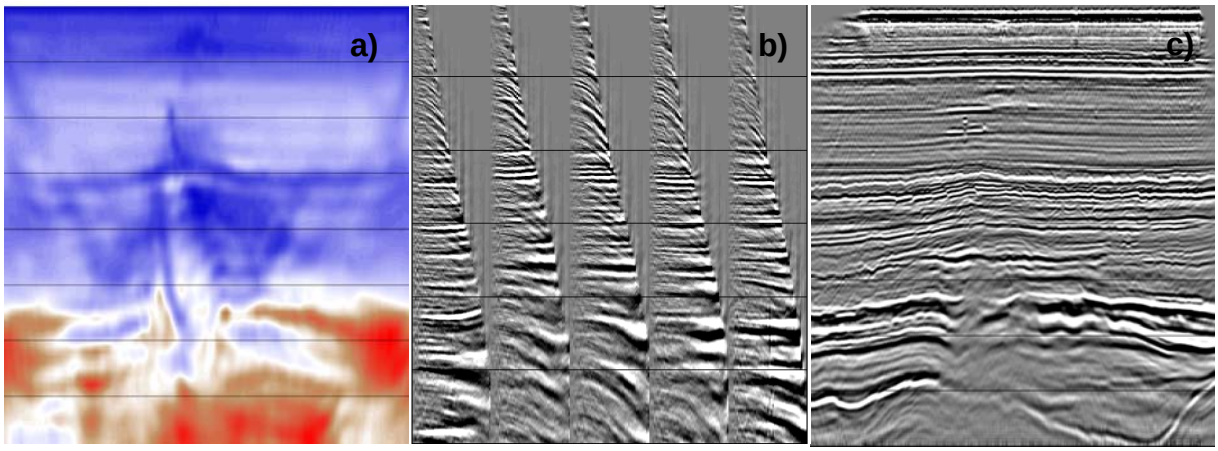

Fig 3: a) One inline section in the velocity model after FWI; b) some common imaging gathers of Kirchhoff migration using the FWI model; c) the migrated section using the FWI inverted model.

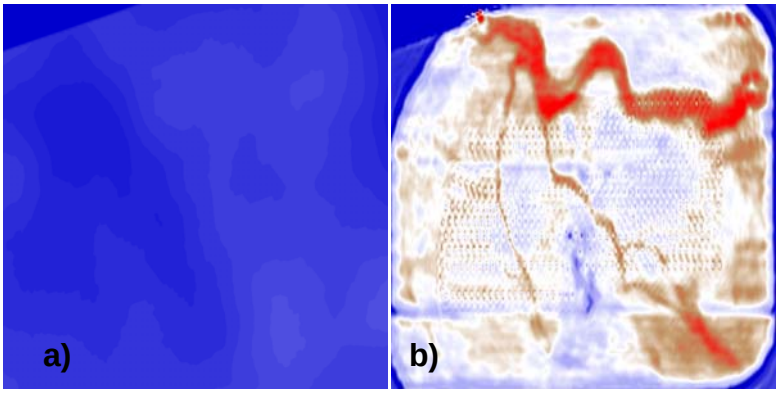

Fig 4: a), a depth slice of the initial velocity model at a shallow depth below the sea surface; b) the same depth slice in the velocity model after FWI, in which clear channels are observed.

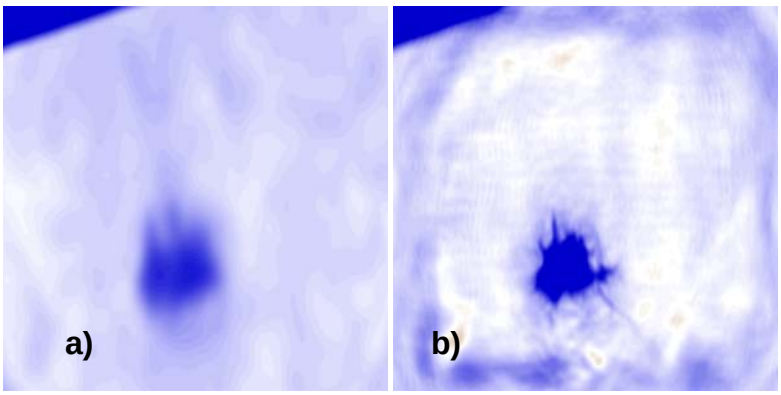

Fig 5: a), a depth slice of the initial velocity model at a deeper part of the earth; b) the same depth slice in the velocity model after FWI, in which the gas cloud is delineated clearly, but the boundary is not clear in the initial model. Both features shown in Fig 4b and Fig 5b are consistent with those in frequency domain FWI results.

DOI http://dx.doi.org/10.1190/segam2012-1105.1

http://dx.doi.org/10.1190/segam2012-1105.1

EDITED REFERENCES

Note: This reference list is a copy-edited version of the reference list submitted by the author. Reference lists for the 2012 SEG Technical Program Expanded Abstracts have been copy edited so that references provided with the online metadata for each paper will achieve a high degree of linking to cited sources that appear on the Web.

REFERENCES

Barkved,O., U. Albertin, P. Heavey, J. H. Kommedal, J.-P. van Gestell, R. Synnøve, H. Pettersen, C. Kent, 2010, Business impact of full-waveform inversion at Valhall: Presented at the 80th Annual International Meeting, SEG.

Bunks, C., F. M. Saleck, S. Zaleski, and G. Chavent, 1995, Multiscale seismic waveform inversion: Geophysics, **60**, 1457–1473.

Landa, E., W. Beydoun, and A. Tarantola, 1989, Reference velocity model estimation from prestack waveforms: Coherency optimization by simulated annealing: Geophysics, **54**, 984–990.

Ma, X., 2001, A constrained global inversion method using an over-parameterized scheme: Application to poststack seismic data: Geophysics, **66**, 613–626

Prieux, V., R. Brossier, J. H. Kommendal, O. I. Barkved, S. Operto, and J. Virieux, 2010, Application of 2D acoustic frequency-domain full-waveform inversion to OBC wide-aperture data from the Valhall field: Presented at the 80th Annual International Meeting, SEG.

Sen, M. K., and P. L. Stoffa, 1991, Nonlinear one-dimensional seismic waveform inversion using simulated annealing: Geophysics, **56**, 1624–1638.

Sirgue, L., O. I. Barkved, J. P. V. Gestel, O. J. Askim, and J. H. Kommedal, 2009, 3D waveform inversion on Valhall wide-azimuth OBC: 71st Annual International Conference and Exhibition, EAGE, Expanded Abstracts, U038.

Stoffa, P. L., and M. K. Sen, 1991, Nonlinear multiparameter optimization using genetic algorithms: Inversion of plane-wave seismograms: Geophysics, **56**, 1794–1810.

Vigh, D., and E. W. Starr, 2008, 3D prestack plane wave, full waveform inversion: Geophysics, **73**, no. 5, VE135–VE144.

Virieux, J., and S. Operto, 2009, An overview of full-waveform inversion in exploration geophysics: Geophysics, **74**, no. 6, WCC1–WCC26.

Warner, M., I. Stekl, and A. Umpleby, 2008, 3D wavefield tomography: Synthetic and field data examples: Presented at the 78th Annual International Meeting, SEG.